Ferroelectric Control of Magnetism in Ultrathin $HfO_2\backslash Co\backslash Pt$ Layers

Bart F. Vermeulen,[*,†,‡] Florin Ciubotaru,[‡] Mihaela I. Popovici,[‡] Johan Swerts,[‡] Sébastien Couet,[‡] Iuliana P. Radu,[‡] Alexandru Stancu,[¶] Kristiaan Temst,[§] Guido Groeseneken,[‖,‡] Christoph Adelmann,[‡] and Koen M. Martens[†,‡]

†*Laboratorium voor Halfgeleiderfysica, KU Leuven, Leuven, Belgium*

‡*IMEC, Kapeldreef 75, Leuven, Belgium*

¶*Faculty of Physics, Alexandru Ioan Cuza University of Iasi, Iasi 700506, Romania*

§*Instituut voor Kern- en Stralingsfysica, KU Leuven, Leuven, Belgium*

‖*Department of Electrical Engineering, KU Leuven, Leuven, Belgium*

E-mail: bart.vermeulen@imec.be

Abstract

The recent demonstration of ferroelectricity in ultrathin HfO_2 has kickstarted a new wave of research into this material. HfO_2 in the orthorhombic phase can be considered the first and only truly nanoscale ferroelectric material that is compatible with silicon-based nanoelectronics applications. In this communication, we demonstrate the ferroelectric control of the magnetic properties of cobalt deposited on ultrathin aluminum-doped, Atomic Layer Deposition-grown HfO_2 (t_{HfO_2} = 6.5 nm). The **ferroelectric effect is shown** to control the shape of the magnetic hysteresis, **quantified here** by the magnetic switching energy. Furthermore, the magnetic properties such as the remanence are modulated by up to 41%. **We show that this modulation does not only correlate with the charge accumulation at the interface but**

also shows an additional component associated with the ferroelectric polarization switching. An in-depth analysis using First Order Reversal Curves shows that the coercive and interaction field distributions of cobalt can be modulated up to respectively 5.8% and 10.5% with the ferroelectric polarization reversal.

Keywords

American Chemical Society, LaTeX

1 Introduction

The effort for scaling ferroelectric materials reached a turning point with the demonstration of ferroelectricity in doped HfO_2 ultrathin films[1–4] ($t_{HfO_2} < 10$ nm). The addition of dopants such as Si,[1,5] Y,[2] Al[3] or Gd[4] distorts the HfO_2 lattice, resulting in an orthorhombic crystal structure.[4,5] In the orthorhombic unit cell, the coordinated displacement of four oxygen ions leads to ferroelectric polarization,[6] which can reach 53 $\mu C/cm^2$ in saturation. In other ultrathin film ferroelectrics such as $BaTiO_3$ or $SrTiO_3$, the Curie temperature is typically very low,[7] unless the material is under significant epitaxial strain from a template layer.[8–10] In addition, the bandgap of Sr(Ba)TiO_3 is particularly low compared to that of HfO_2[11–13] leading to high leakage currents when an electric bias is applied. Furthermore, the interfacial dielectric dead layer, common between Sr(Ba)TiO_3 and electrode metals,[14] has lower permittivity and lowers the voltage drop across the ferroelectric. This dead layer can be suppressed through interfacial engineering in HfO_2.[15] HfO_2 offers the prospect of growing ultrathin layers that are ferroelectric at room temperature (with T_{Curie} up to 450°C)[16] without recourse to epitaxial strain from a template layer. All three of these requirements are crucial for the compatibility of this ferroelectric layer with truly nanoscale electronic devices and applications. Room temperature ferroelectric behaviour has been demonstrated in X:HfO_2 (with X = Si, Al, Y, Gd, La and Sr) down to $t_{HfO_2} < 10$ nm[17] and Y:HfO_2 has

been shown to be ferroelectric down to 3 nm.[18] Furthermore, stoichiometric $Hf_{0.5}Zr_{0.5}O_2$ has recently been demonstrated to be ferroelectric for layers as thin as 2.5 nm.[19] Finally, doped HfO_2 layers can be deposited using Atomic Layer Deposition (ALD),[20] which makes the fabrication compatible with highly scaled Si CMOS technology nodes.

Electrical manipulation of the ferromagnetic properties of **metallic** thin films has been an area of intensive research for the past years. The prospect of modulating a magnetic state without using an energetically expensive Oersted field or spin-polarized current would clear the way for many magnetic alternatives to electronic technologies. Five different mechanisms can be distinguished: single phase multiferroicity,[21–23] modulation of interfacial bonding states,[24] strain-driven modulation,[25–27] ionic motion[28–30] and charge accumulation at a ferromagnet-dielectric interface, a mechanism frequently ascribed to the Voltage Control of Magnetic Anisotropy effect, VCMA.[31–34] Charge driven magnetoelectric phenomena such as VCMA in ultrathin film bilayers using dielectrics can be fast and fully reversible. **Until now, VCMA has been demonstrated using MgO as a dielectric, [31–34] and in some particular cases $SrTiO_3$[35] and $MgAl_2O_4$.[36] The condition of the insulator/ferromagnet interface is crucial, and so far MgO has proven to be the most convenient dielectric. In addition, the strength of charge driven anisotropy modulation has so far been of limited usefulness for electronics applications.[34]**

Ferroelectric control of magnetism has been demonstrated as well: relying on polymer ferroelectrics,[37,38] multiferroic layers such as $BiFeO_3$ requiring a particular epitaxial template,[21–23] or crystalline ABO_3 layers such as $BaTiO_3$ that are either too thick[7,39,40] or have a low Curie Temperature[7] unless they are strained by a monocrystalline template layer unsuitable for Si based nanoelectronics applications.[10,41]

The dominant theory for charge driven control of magnetic anisotropy[31,32,42]

predicts that a ferroelectric layer should effect non-volatile control of the magnetic properties of a ferromagnetic metal. To validate this prediction using fully CMOS-compatible materials, a ferroelectric layer needs to be selected which promotes an excellent with a ferromagnetic metal layer. In the field of room temperature ferroelectric control of ferromagnets, the potential of HfO_2 has yet to be demonstrated. In this communication, we demonstrate the ferroelectric control of the magnetic properties of ultrathin CoPt films at an interface with HfO_2.

2 Results and Discussion

2.1 Magnetization, structure and morphology of the HfO_2\Co\Pt stack

For this study, we use a Co (0.45 nm)\Pt (5 nm) bilayer deposited on a 6.5 nm Al-doped HfO_2 layer. **The HfO_2 layer is intended to be as thin as possible, while retaining suitable ferroelectric and insulating properties. A thicker ALD-grown HfO_2 layer, with $t_{HfO_2} = 8$ nm or above may show better material quality, and therefore better ferroelectric properties[18,20]. However, here we intend to demonstrate ferroelectric control under conditions closely compatible with CMOS operation; this means thin ferroelectrics and low voltages. Furthermore, the dopant which distorts the HfO_2 lattice is chosen to be Al due to its common availability in ALD systems. Other dopants such as Gd, Zr or in particular La have been shown to improve the ferroelectric properties compared to Al[17,43], and in particular La-doped $Hf_{0.5}Zr_{0.5}O_2$ combines high endurance and remanent polarization[43,44]. These alternative dopants provide perspective for future work on ferroelectric VCMA.**

The presence of the orthorhombic phase of HfO_2 is crucial for the ferroelectric order[4–6]

and is confirmed by Grazing Incidence X-Ray Diffraction (GIXRD, see Figure 1.**a**). The peaks at 2θ angles of 30.4° and 34.5°[45,46] show that the crystal structure of HfO_2 is mixed between orthorhombic and cubic, as expected from the state of the art.[20] The peak at 34.5° originates solely from the orthorhombic (111) plane, and demonstrates the presence of this phase. A quantitative phase analysis is prevented by the overlap of GIXRD peaks of the different HfO_2 phases. **An additional, broad XRD peak centered around 41.1° shows the presence of intermixed fcc (111) Co and Pt.[47,48] The thin Co layer has interdiffused with its Pt cap, and adopted the same fcc (111) structure. The intermixing of Co and Pt is also evident from the Energy-Dispersive X-Ray Spectroscopy (EDS) analysis in Figure 1.b. Henceforth, given that the magnetic Co layer has interdiffused with its Pt cap, Co\Pt refers to the as deposited layer, and CoPt to the interdiffused layer where the ferroelectric control takes place.**

All ferroelectric materials are also piezoelectric.[49] It is therefore important to ensure that magnetoelectric effects in HfO_2\CoPt are due to the ferroelectric polarization of HfO_2 and not piezoelectric strain. First, the piezoelectric displacement in HfO_2 is at least an order of magnitude smaller than typical piezoelectric materials,[1] so any strain-driven effect would likely be particularly weak. Furthermore, it is crucial to ascertain that the interface between Al:HfO_2 and Co is free of any residual layers, to ensure that the Co surface is impacted by the ferroelectric polarization of HfO_2 and not by strain transferred through a residual layer. Energy-Dispersive X-Ray Spectroscopy (EDS) analysis shows that the HfO_2\Co interface is slightly interdiffused and free of contamination (Figure 1.**b**). In particular, the absence of residual TiN is shown. A TiN sacrificial layer is used during HfO_2 crystallization[20] and needs to be replaced with the magnetic Co layer (see Supplementary Material). The clean HfO_2\Co interface and the relative weakness of the piezoelectric displacement[1] reliably minimize the possible impact of piezostrain.

The polycrystalline structure of HfO_2 is shown with High-Resolution Transmission Electron Microscopy (HRTEM, Figure 1.**c**). The grain size is estimated to be around 10 nm, and is not directly determined by the grain size or orientation of the underlying TiN layer (Figure 1.**d**). The Co layer cannot be seen in HRTEM due to significant interdiffusion between Co and Pt, as seen with EDS and GIXRD (see Supplementary Material), and it is therefore more accurate to consider the interdiffused Co\Pt layer as the magnetic layer. **This interdiffusion is a consequence of the thermal anneal applied after the Co\Pt\Ru deposition[48].**

Finally, the thicknesses of the different layers are derived from TEM, and confirmed with Rutherford Backscattering Spectroscopy (RBS) analysis (see Supplementary Material). From RBS, the as-deposited Co thickness of the samples used in the following paragraphs is measured: $t_{Co} = 0.45 \pm 0.02$ nm.

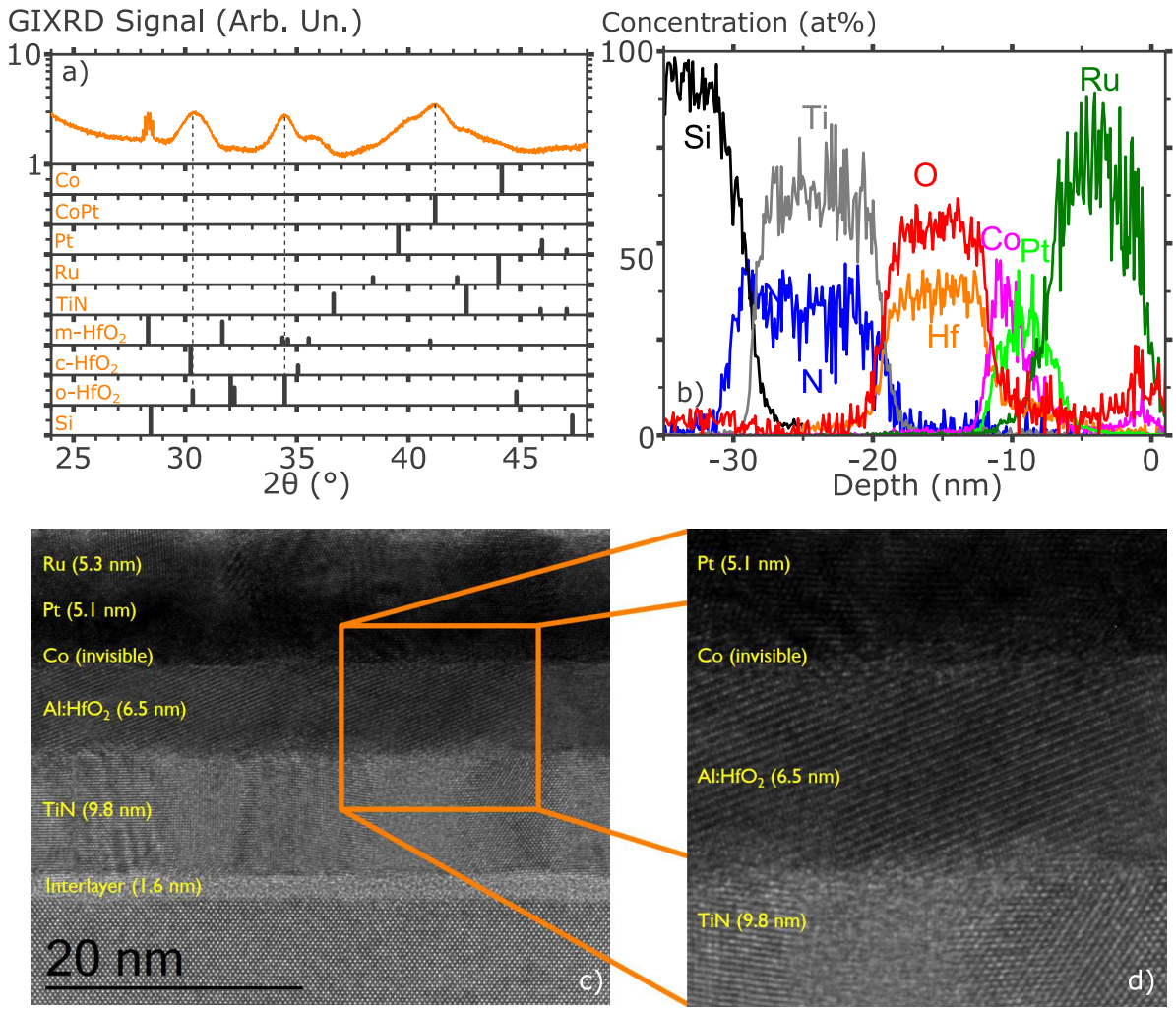

Figure 1: **a)** The Grazing Incidence X-Ray Diffraction characteristic of the materials stack shows the presence of the orthorhombic HfO_2 phase. **b)** Energy Dispersive X-Ray Spectroscopy shows the atomic concentration versus depth in the sample. **c)** Transmission Electron Microscopy image of the materials stack and **d)** zoom. The TEM/EDS image is captured on a sample with a thick Cobalt layer, to illustrate interdiffusion.

The deposited thickness of the Co layer and the Pt cap are chosen to orient the magnetization perpendicular to the sample plane (perpendicular magnetic anisotropy, PMA).[48,50,51] **As mentioned earlier in the discussion of the GIXRD and EDS results, the Co and Pt layer have significantly interdiffused upon thermal annealing. It is therefore more accurate to consider an fcc (111) alloyed CoPt layer with a Pt cap as the magnetic layer.** The magnetic properties of this CoPt layer are probed using vibrating sample magnetometry (VSM). The dependence of the magnetic moment on the deposited

Co thickness can be seen in Figure 2.**a**. The magnetization of the sample M = 1.42 ± 0.07 MA/m (see Supplementary Material) is comparable to the magnetization of bulk cobalt (1.44 MA/m).[52]

A sharp Co/Pt interface, such as in a Co/Pt superlattice or a Co\Pt layer deposited on a thick, crystalline Pt template layer, typically shows strong PMA[53,54]. However, in the case of an interdiffused Co/Pt interface or even a CoPt alloy, PMA can be obtained by promoting the fcc (111) crystalline structure[55]. In fact, in Co\Pt bilayers deposited on an oxide, such as SiO_2 or amorphous HfO_2, a thermal annealing step is necessary to induce PMA in the magnetic layer[48,56]. This annealing process leads to interdiffusion on the one hand, and to crystalline reordering of the CoPt lattice under the influence of the fcc (111) Pt layer. In this material stack, the CoPt layer is shown to have an fcc (111) structure from the XRD peak at $2\theta = 41.1^\circ$ (Figure 1.a).[48] The materials stack shows PMA up to a deposited cobalt thickness (t_{Co}) of 1.75 nm (Figure 2.**b**). In the PMA regime, the effective anisotropy K_{eff} saturates at 0.12 ± 0.033 mJ/m^2 (Figure 2.**b** and see Supplementary Material).

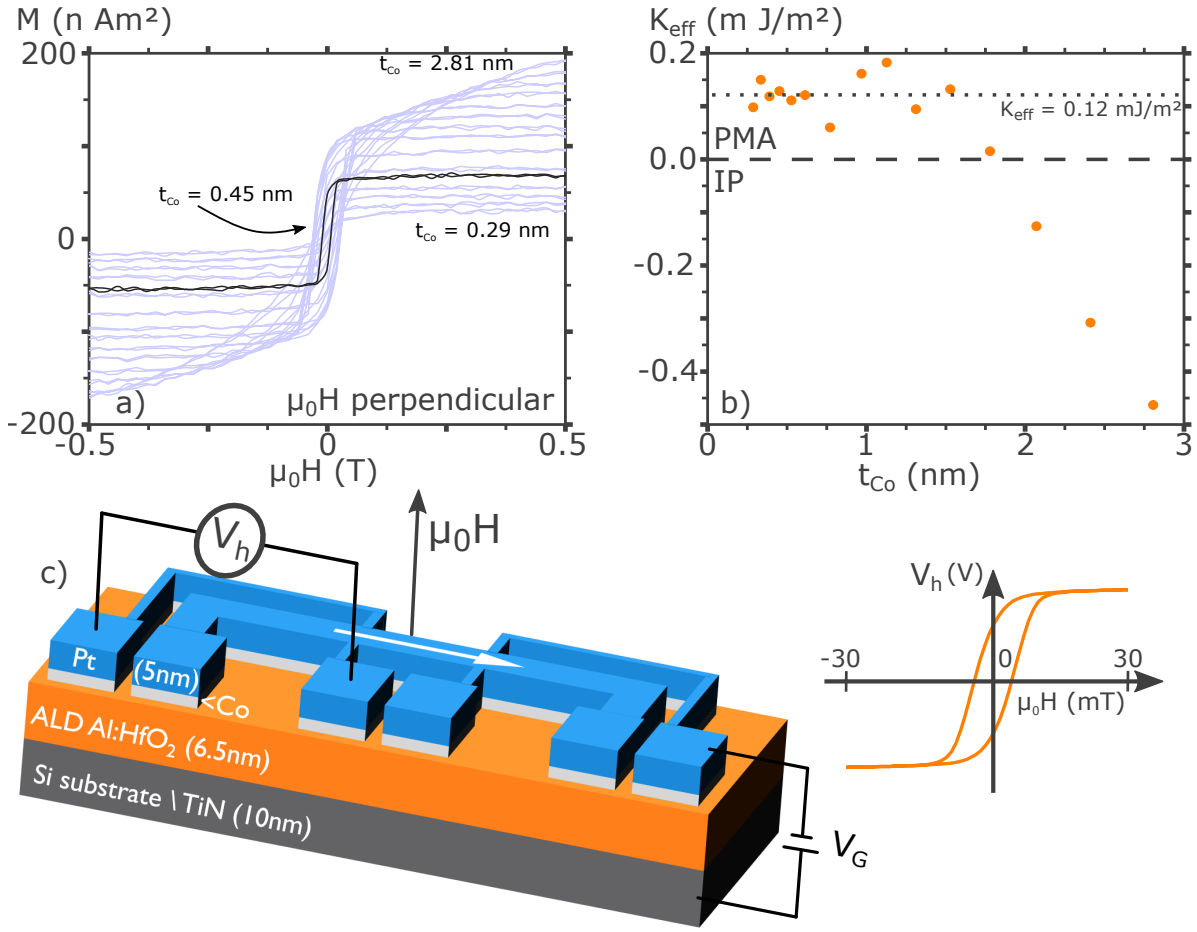

Figure 2: **a)** The magnetization curves measured using VSM for increasing t_{Co} with out-of-plane applied magnetic field (in dark grey the magnetization curve of the sample discussed henceforth). **b)** Thickness dependence of the effective magnetic anisotropy energy K_{eff}. By convention, $K_{eff} > 0$ indicates perpendicular magnetic anisotropy (PMA). **c)** The Hall bar design used for the electrical measurements. The applied gate voltage V_G, the measured Hall voltage ("V") and the channel current (white arrow) are indicated. The inset shows an anomalous Hall Effect measurement with out-of-plane μ_0H.

2.2 Ferroelectric training and characterization

Thin film ferroelectric materials typically do not exhibit ferroelectric ordering as-deposited,[3] but instead need to be electrically trained. Training of ferroelectrics consists of repeatedly cycling the applied voltage, in order to align the different ferroelectric domains parallel to each other. The effect of training is shown in Figures 3.**a** and **b**. Before training, the reversal current through the ferroelectric shows a typical dielectric current-voltage curve.

The ferroelectric behaviour is characterized by switching events seen as peaks in the I-V relationship. As the ferroelectric is trained, the switching events merge into a single, broad ferroelectric polarization switch at the coercive voltage (Figure 3.**a**). The polarization of HfO_2 consists of the net amount of electrical charge displaced inside the ferroelectric layer, and equals the amount of charge accumulated in the electrodes of the ferroelectric capacitor. After cycling, the polarization shows the typical ferroelectric hysteresis behaviour (Figure 3.**b**). The HfO_2 layer reaches a polarization $2P_r = 14\ \mu C/cm^2$. This value is lower than our previously reported figures ($27\ \mu C/cm^2$),[20] this is explained by the difference with respect to the original process, i.e. replacing the top electrode with cobalt.

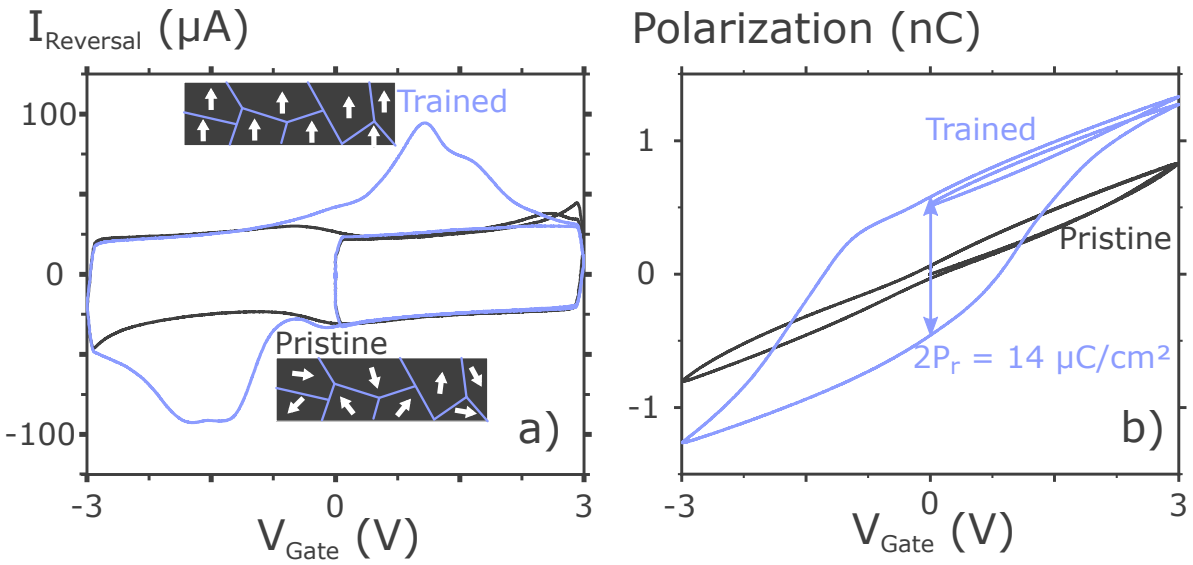

Figure 3: **a)** The current through Al:HfO_2 versus V_G in square capacitors (90 μm side) show the ferroelectric polarization switching events as a peak in the reversal current. **b)** The polarization of the ferroelectric layer obtained from integrating the current in **a**. Training leads to opening of the hysteresis loop. The double arrow indicates the remanent polarization $2P_r$.

2.3 Ferroelectric control of the magnetic hysteresis

The magnetization of the samples is measured electrically with the anomalous Hall effect (AHE) using a Hall bar device (shown in Figure 1.**c**). A current is applied in the plane, along the channel. The gate voltage V_G is applied between the top Ru electrode and the bottom

Si electrode, and the magnetic field is applied out of the plane. The Hall voltage V_{Hall} is measured across one of the two Hall crosses present along the channel. The ferromagnetic hysteresis loop is measured with the anomalous Hall effect as a function of the applied gating voltage V_G. The used V_G sequence is shown in the inset of Figure 4.**a**.

The impact of the gating voltage on the ferromagnetic hysteresis amounts to a gradual change in the shape of the loop for pristine HfO_2 (Figure 4.**a**). For trained HfO_2, two distinct states appear in the voltage-dependent ferromagnetic hysteresis loops, corresponding to the two ferroelectric states (see Figure 4.**b**). The positive gating voltage in the pristine sample, or positive ferroelectric polarization in the trained sample leads to a flatter, less square magnetic hysteresis loop. The trained sample is characterized further by recording the magnetic remanence versus the gate bias V_G, and a reproduction of the ferroelectric hysteresis loop is obtained (Figure 4.**c**). In the trained state, the magnetic remanence can be modulated by the ferroelectric polarization by up to 7.8 μV in terms of the Hall voltage or 41%. During training, the quasi-linear dependence of $V_{Hall,remanence}$ on V_G opens up to reproduce the ferroelectric hysteresis loop which is shifted to lower $V_{Hall,remanence}$ values. After training, the electrical control of the magnetic properties is strongly enhanced and the magnetic properties are shifted irreversibly. As training of the HfO_2 layer leads to a change from the dielectric to the ferroelectric phase, the interface with CoPt is impacted as well, leading to a change in the CoPt magnetic properties. Several phenomena have been associated with the emergence of the ferroelectric ordering through training:[20] formation of an oxide layer between an electrode and HfO_2,[57] phase transitions,[58,59] presence of an internal bias due to mobile ions[60] or the redistribution of oxygen vacancies.[61] Hence it is most likely that changes to the HfO_2 bulk and interface impact the magnetic properties of the CoPt layer, and justify the downward shift seen in the magnetic remanence. Despite this shift upon training the ferroelectric layer, the HfO_2 ferroelectricity, as evidenced by the magnetic properties, is retained reliably for up to 10^7 fast switching cycles (see Supplemen-

tary Material). To summarize, the shape of the magnetic hysteresis loop as evidenced by the magnetic remanence is determined by the ferroelectric polarization hysteresis loop, and demonstrates ferroelectric control of magnetism in HfO_2\CoPt.

In the most common explanation for VCMA,[31–34] the electrical charge accumulation at the interface between a dielectric (here, the ferroelectric) and a ferromagnetic material leads to a change in the effective magnetic anisotropy energy K_{eff}. The magnetic anisotropy, which depends on the polarization of the ferroelectric capacitor as expected for the charge accumulation mechanism, can be determined from the ferromagnetic hysteresis shape. In reality, the magnetization curve for a PMA sample may not be perfectly square, and the magnetization switching may not happen abruptly at a single H_c, but gradually. The magnetic non-uniformity of the sample prevents a straightforward quantitative computation of K_{eff}, as would be required to quantify the VCMA effect. Therefore, we derive the Magnetic Switching Energy, which is a measure for the magnetic energy spent in switching the magnetization of the sample:

$$MSE \ \ (T\,V) \ = \int_0^{V_{Hall,Sat}} \mu_0 H \; dV_{Hall} \tag{1}$$

The MSE of Equation 1, as a qualitative measure for anisotropy, is expected to be dependent on the ferroelectric polarization through VCMA. Therefore, in both the pristine and the trained state, the MSE dependence on the gating voltage V_G should reliably reproduce the ferroelectric polarization of Figure 3.**b**.

As can be seen in Figure 4.**d**, in the pristine state, the MSE shows the same quasi-linear dependence on V_G as the polarization; conversely, in the trained state, the ferroelectric hysteresis loop is evident in the MSE, along with the shift ascribed to training. The clear correlation between the dependence of the MSE on the gating voltage and the ferroelectric

polarization shows that in this HfO_2\CoPt layer, the ferroelectric and ferromagnetic states are coupled.

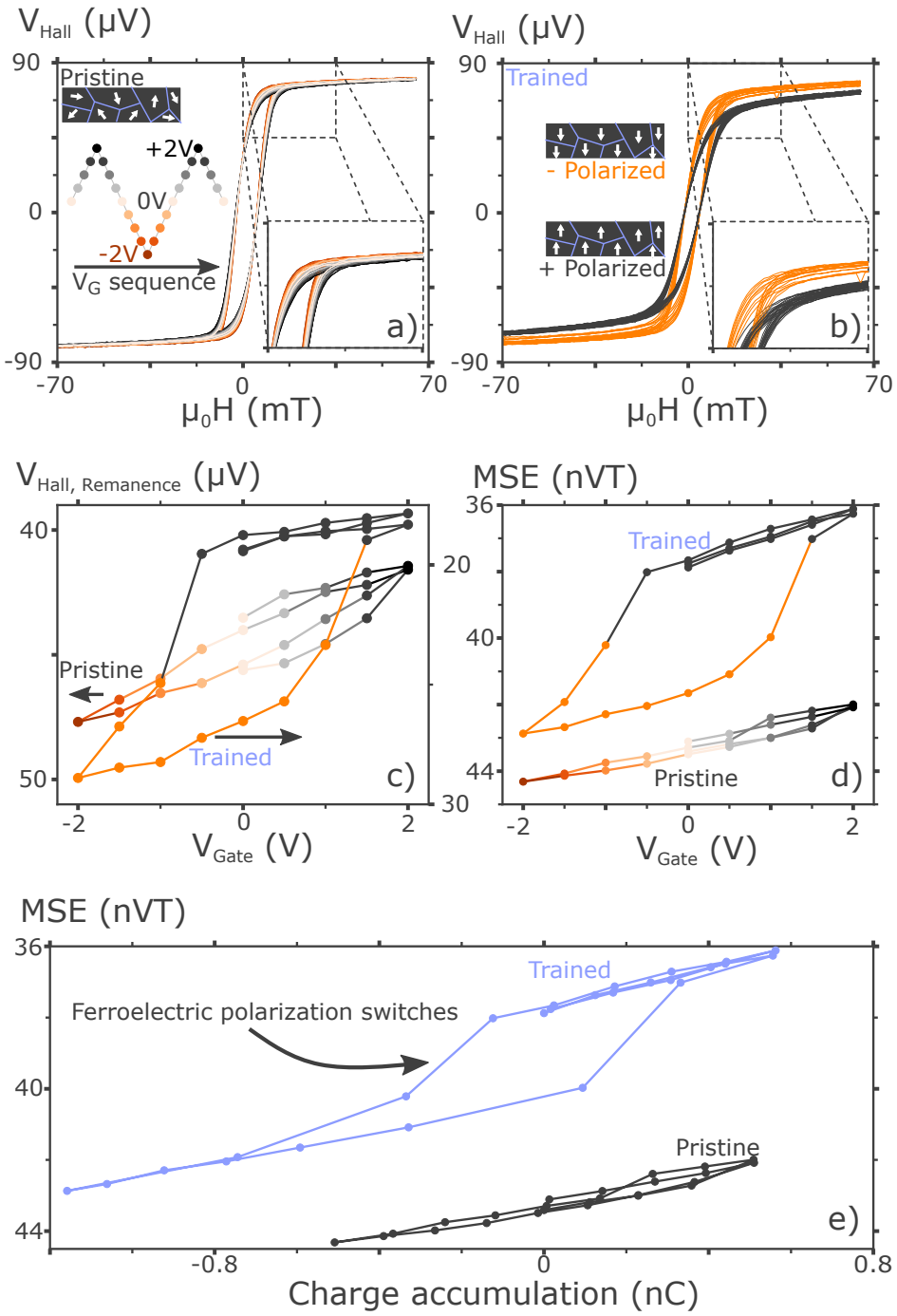

Figure 4: **a)** The sequence of V_{Gate} as applied in the voltage control experiments (inset) and the anomalous Hall effect curves **at each gating voltage** before ferroelectric training. **b)** After ferroelectric training, two distinct states arise corresponding to the ferroelectric polarization. The insets in **a** and **b** show a zoom into the remanent part of the measurement. **c)** The magnetic remanence versus the gate voltage and **d)** the magnetic switching energy (MSE, eq 1) versus gate voltage. Both characteristics show that as the samples go through ferroelectric training, the ferroelectric hysteresis is reproduced in the remanence and MSE, demonstrating ferroelectric control of the magnetic properties of CoPt. **e)** The relationship between the accumulated charge and the MSE reveals a charge- and a polarization-dependence.

From this similarity between the electric field-dependence of the magnetic remanence and the ferroelectric polarization, we deduce the modulation mechanism at play in this materials stack to be intrinsic to the ferroelectric/ferromagnet interface: the modulation of interfacial bonding states[24] or the charge accumulation mechanism most commonly deemed responsible for VCMA,[31–34] or a combination of both. A careful examination of the dependence of the MSE on the accumulated charge further sheds some light on the underlying mechanism (Figure 4.**e**). For a charge accumulation mechanism, the dependence of the magnetic properties on the accumulated charge is expected to show a continuous behaviour. In fact, the charge-dependence is often shown to be linear,[31,34] and accordingly we observe such linear dependence for the untrained HfO_2 layer (Figure 4.**c, d**). However, in the trained sample, an abrupt transition is observed in the MSE versus accumulated charge as the ferroelectric polarization switches. This additional component provides evidence that a charge accumulation mechanism alone cannot fully account for the encountered behavior and that **the modulation of interfacial bonding states[24] plays a role as well**.

2.4 FORC analysis

To complement the analysis based on the magnetic hysteresis, the coercivity of the magnetic layer, and more precisely its distribution in this non-uniform sample, is probed using a First Order Reversal Curves (FORC) analysis. The FORC analysis assumes that a non-uniform sample consists of many elementary magnetic particles, called Hysterons. The Hysteron is defined by two parameters: the coercive field H_c which represents the width of the hysteresis loop, and the interaction field H_i which can be seen, empirically, as the shift of the Hysteron along the magnetic field axis (inset of Figure 5.**a**). Physically, the interaction field arises from the proximity of other magnetic particles around a Hysteron, e.g. through magnetic exchange or dipolar fields. The FORCs are measured at $V_G = 0$ V, after polarizing the ferroelectric with a voltage pulse of either +3 V or -3 V (the negative ferroelectric polarization is shown in Figure 5.**a**). Measuring the FORCs in ferroelectric remanence ensures that the

changes in the FORC distribution are exclusively due to the remanent polarization of the ferroelectric HfO_2. In ferroelectric materials like HfO_2, the lattice strain in remanence is essentially zero, which rules out strain as a modulation mechanism altogether.[1]

The magnetization of the sample is collected as a function of the applied field $\mu_0 H$ and the reversal field $\mu_0 H_R$ according to the FORC protocol.[62] A FORC curve is obtained when the magnetic field sweep is interrupted at the reversal field $\mu_0 H_R$, and subsequently reversed, back to positive saturation (Figure 5.**a**). The FORC distribution ρ shows the distribution of the properties of the Hysterons (defined by H_c and H_i) in H_c-H_i space. In essence, the FORC distribution ρ tells us how many Hysterons are present in a sample, with a given H_c and H_i (Figure 5.**d**). The FORC distribution ρ is calculated from the FORC measurement as the second derivative of the magnetization (normalized to $V_{Hall,Saturation}$) to the applied field and the reversal field:[62]

$$\rho\left(H, H_R\right) = -\frac{1}{2}\frac{\partial^2 m_{FORC}\left(H, H_R\right)}{\partial H \partial H_R} \tag{2}$$

Two features stand out in the FORC distribution (Figure 5.**d**): a wide peak at low $\mu_0 H_c$ and positive $\mu_0 H_i$; and a peak centered around $\mu_0 H_i$ = -1.8 mT and $\mu_0 H_c$ = 5.5 mT, indicated with an "**x**". The first peak is ascribed to kinetic effects that may be related to magnetic domains with a narrower distribution of coercive fields.[63] In these domains, the magnetization has been shown to relax to its equilibrium position in a timescale that is longer than that of the experiment.[63] Due to this longer relaxation timescale, the ferroelectric polarization does not visibly impact the distribution of these domains. The second peak reflects the properties of the ferromagnetic domains present in the CoPt layer that are impacted by the ferroelectric polarization of HfO_2. A cross-section of this peak is shown versus the coercive field H_c and the interaction field H_i respectively in Figure 5.**b** and 5.**c**. The cross sections of the FORC distribution along both field axes are fitted with a Gaussian function to extract

the position of the center σ and the width of the peak μ.

The distribution of the coercive field H_c (Figure 5.**b**) shifts to higher fields for positive ferroelectric polarization (taking negative polarization as the reference), but also broadens significantly. The center of the coercive field peak shifts with 0.32 mT; an increase of 5.8% ascribed to a change in the magnetic anisotropy through VCMA.[64] Interestingly, the width of the H_c distribution also increases, with 0.8 mT or 13%. The fact that the width of the distribution is impacted by the ferroelectric polarization shows that the modulation of the magnetic properties is nonuniform, just like the magnetic properties themselves. Finally, the center of the H_i peak shifts by 0.19 mT or 10.5% and its width by 0.37 mT or 10.4% as the ferroelectric polarization switches.

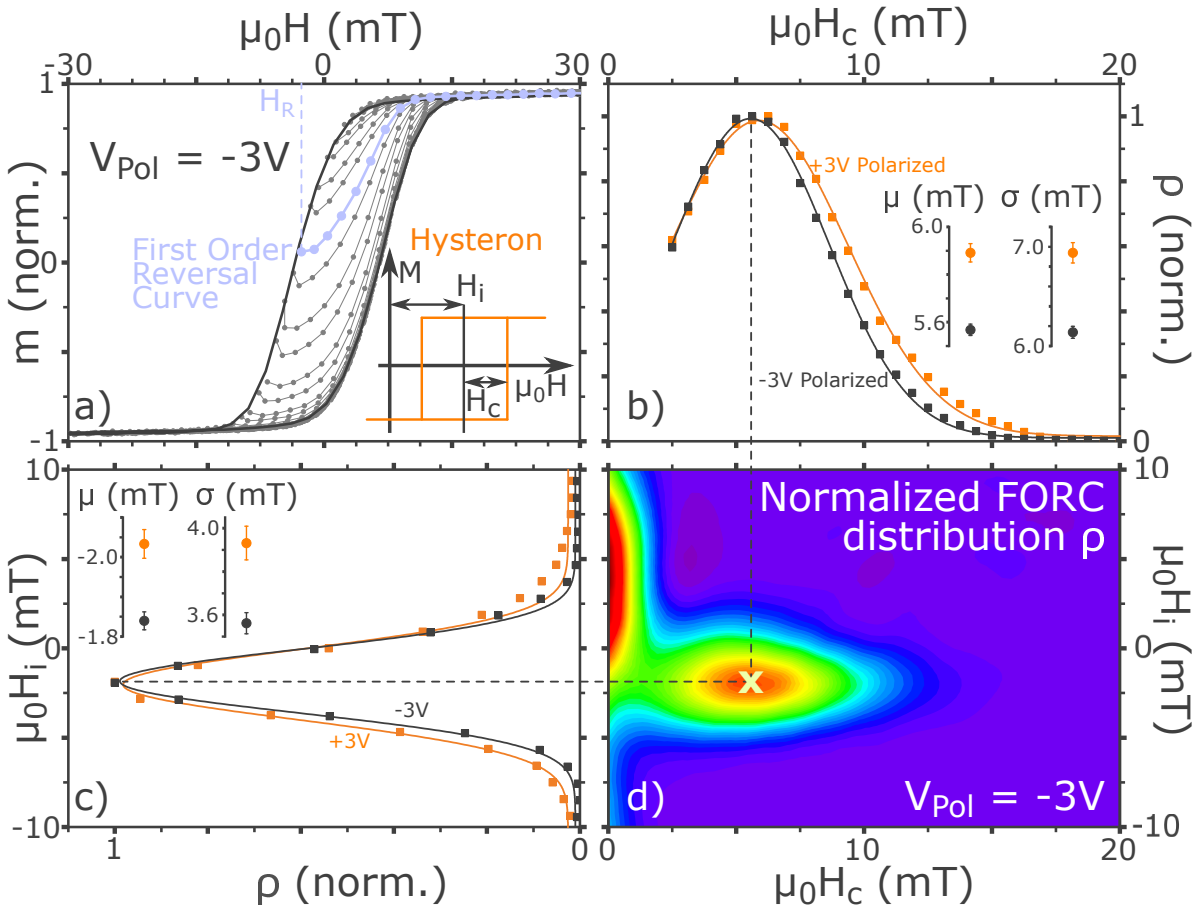

Figure 5: **a)** A FORC measurement comprises the set of curves from the reversal field H_R to the saturation field $\mu_0 H = 40$ mT; the goal is to extract the distribution of properties of the hysterons in the sample (inset). An individual FORC is shown in light blue. **b)** and **c)** The cross sections of ρ along the coercive field and interaction field axes show the modulation due to the ferroelectric polarization. The dots represent the FORC distribution ρ and the lines are Gaussian fits to the data. The center position of the Gaussian peak μ and its width σ are shown in the insets. **d)** The FORC distribution ρ is calculated using eq. 2.

In the following final paragraphs, we place the effect reported here into the broader context of voltage control of magnetism[65,66] using three selected reference materials: ferroelectric polymer P(VDF-TrFE), solid-state ferroelectric $BaTiO_3$ and solid-state multiferroic $BiFeO_3$. We provide a quantitative comparison of the strength wherever possible.

First of all, ferroelectric polymer layers have been shown to modify the coerciv-

ity of a thin Co layer.[37,38] For instance, the coercive field of Co deposited on a thick Pt seed can be modulated by up to 16 mT (or about 30%) by the remanent polarization of the ferroelectric polymer P(VDF-TrFE).[38] In comparison, we show a change of 5.8% of the coercivity with the ferroelectric polarization of HfO_2 from FORC. While the effect reported here is weaker than the effect arising from the polymer ferroelectric, the applicability advantage of using a CMOS-compatible solid-state ferroelectric such as HfO_2 outweighs the strength considerations.

The prime example of a solid-state ferroelectric is $BaTiO_3$ (BTO). Sahoo et al.[67] show that the ferroelectric polarization of single crystal BTO can modulate the coercivity of Fe by up to 20% at room temperature. In remanence, this modulation strength is around 4.5%, which is quite comparable to the 5.8% reported in this publication. The major advantage of HfO_2 resides in its thin film, room temperature ferroelectricity and the CMOS-compatible seed-layer material, TiN. In comparison, $BaTiO_3$ is ferroelectric at room temperature in monocrystalline substrates[39,40,67] or fairly thick deposited films.[7] Another option to obtain room temperature ferroelectricity in BTO is to expose it to significant epitaxial strain to increase the ferroelectric Curie temperature[7], using a template layer that is incompatible with Si nanoelectronics.[10,41]

Finally, ferroelectric control of magnetism is also present in single-phase multiferroic materials such as $BiFeO_3$ (BFO). The polarization of BFO is for instance shown to control the coercive field of $La_{0.7}Sr_{0.3}MnO_3$ by up to 50 mT or around 100% at 5.5 K.[68,69] Single-phase multiferroic layers exhibit many interesting physical phenomena. However, these materials, such as BFO broadly suffer from the same issue as BTO and related ferroelectric layers concerning the re-

quired crystalline quality for CMOS-compatibility. BFO shows multiferroicity and control of the magnetic properties in typically thick layers (around 100 nm) and deposited on CMOS incompatible seed layers such as $SrRuO_3$[21–23].

Ferroelectric control of magnetism using fully CMOS-compatible materials stack had never been shown. Here, the ferroelectric HfO_2 layer is ultrathin and has a high Curie temperature, and the TiN template layer is compatible with nano-electronics processing.

3 Conclusion

In summary, we demonstrate ferroelectric control of the magnetic properties of in a HfO_2\CoPt trilayer. The ferroelectric material is a solid state, 6.5 nm thick layer of ALD grown Al:HfO_2. The polarization of the ferroelectric layer impacts the shape of the magnetic hysteresis, characterized by the magnetic switching energy. Furthermore, the magnetic properties such as the magnetic remanence can be modulated with up to 41% with the ferroelectric polarization. **In addition, we show that magnetic properties are modulated through two distinct mechanisms: the accumulated charge and the ferroelectric polarization itself.** A First Order Reversal Curves (FORC) analysis of the magnetic layer also shows the modulation by the ferroelectric polarization in the distribution of coercivity and interaction fields. Using the positive and negative ferroelectric remanent states, the center of the H_c and H_i distributions can be modulated up to respectively 5.8 and 10.5%. Just as ferroelectricity in HfO_2 kickstarted a new wave of research in the application of ferroelectric materials in microelectronics, these results open a new path to the application of thin film ferroelectric materials in advanced spintronics and MRAM applications.

4 Experimental Section

Samples are fabricated on Si wafers after an O_3 based clean leaving 1 nm of amorphous SiO_2. A forming gas anneal at 420°C for 20 minutes is applied to passivate dangling bonds, after which 10 nm of TiN is sputter deposited. 6.5 nm of ferroelectric Al:HfO_2 was deposited by atomic layer deposition at 300°C using hafnium chloride $HfCl_4$ and trimethylaluminum $Al(CH_3)_3$ as metal precursors and H_2O as the oxidant and with a pulse ratio of Hf:Al = 34:1.[20] A further 10 nm of TiN were deposited, followed by a rapid thermal anneal step at 850°C for 1 min in N_2 at atmospheric pressure to crystallize the FE. The top layer of TiN is removed with an alkaline wet etch using a mixture of NH_4OH, H_2O_2 and de-ionized water, and the samples are transferred to a Canon Anelva EC7800 PVD cluster tool. An in-situ rapid thermal anneal in vacuum is performed at 350°C for 5 minutes prior to the sputter-deposition of the Co thin film with thickness ranging from 0.4 to 2.4 nm. Subsequently, 4 nm of Pt followed by 5 nm of Ru are deposited in-situ on top of Co. Samples are finally annealed at a temperature of 300°C at atmospheric pressure for 10 min in N_2 ambient. After deposition, the samples are patterned into capacitor and Hall Bar structures using Ar^+ ion milling. TEM and energy dispersive X-ray spectroscopy (EDS) specimens are prepared using conventional ion milling and imaged in a FEI Titan at 300kV. Rutherford backscattering spectra (RBS) were obtained using a He^+ beam with an energy of 1.523 MeV, at a scattering angle of 170° and sample tilt angle of 11°. RBS is used to measure the thickness of Co layers at different locations on 300 mm wafers, with an accuracy of 5%. The Co thickness is calculated assuming fcc (111) texture of the Co layer, and has the same accuracy of 5%. Vibrating sample magnetometry (VSM) measurements were performed using a Microsense EV11 tool at room temperature on 8x8 mm^2 samples. The anomalous Hall effect (AHE) measurements are performed in a home-built electrical probing tool equipped with a PHYWE air-cooled magnet. **First Order Reversal Curves (FORC) measurements are measured using the AHE as well, and analyzed using home-built software. FORC measurements are complementary to classical hysteresis loop measure-**

ments and provide a wealth of information concerning the collective behaviour of Preisach-like magnetic domains.[62] The polarization-voltage and current-voltage measurements are performed on a 90 μm square capacitor, using a Keithley 4200 pulsed IV setup and a rise time of 10 μseconds/volt. GIXRD is performed in an X'Pert X-Ray Diffractometer at an incidence angle of 1°.

Acknowledgement

We wish to acknowledge the support J Meersschaut for fruitful discussions on Rutherford Backscattering Spectrometry; H Bender for assisting in the analysis of TEM micrographs and EDS spectra; K Florent for experimental help in measuring the ferroelectric properties of HfO_2; A Stesmans and V Afanasiev for fruitful discussion on ferroelectrics. We acknowledge the financial support of FWO through grant n° G0D5315N, the Concerted Research Action GOA 14/007 and C1-program C14/18/074 of KULeuven. The authors declare no conflict of interest.

Author contributions: BV carried out all the measurements and their analysis, with the exception of the FORC analysis; MP, JS and SC fabricated the materials; AS carried out the analysis of the FORC data; IR and GG provided structural support; KT provided useful feedback on the manuscript; KM provided scientific support for the work and laid out the original ideas; FC and CA provided daily scientific support for the work.

5 Supporting Information Available

Supplementary material is available discussing processing details on the removal of the sacrificial TiN layer; Co thickness through Rutherford Backscattering Spectroscopy (RBS); the magnetic properties through Vibrating Sample Magnetometry (VSM); the derivation of the Magnetic Switching Energy (MSE) method; an investigation of long term pulsed stress; and some experimental notes on the determination of the switching mechanism.

References

(1) Böscke, T.; Müller, J.; Bräuhaus, D.; Schröder, U.; Böttger, U. Ferroelectricity in hafnium oxide thin films. *Applied Physics Letters* **2011**, *99*, 102903.

(2) Müller, J.; Schröder, U.; Böscke, T.; Müller, I.; Böttger, U.; Wilde, L.; Sundqvist, J.; Lemberger, M.; Kücher, P.; Mikolajick, T.; Frey, L. Ferroelectricity in yttrium-doped hafnium oxide. *Journal of Applied Physics* **2011**, *110*, 114113.

(3) Müller, S.; Müller, J.; Singh, A.; Riedel, S.; Sundqvist, J.; Schröder, U.; Mikolajick, T. Incipient ferroelectricity in Al-doped HfO2 thin films. *Advanced Functional Materials* **2012**, *22*, 2412–2417.

(4) Müller, S.; Adelmann, C.; Singh, A.; Van Elshocht, S.; Schröder, U.; Mikolajick, T. Ferroelectricity in Gd-doped HfO2 thin films. *ECS Journal of Solid State Science and Technology* **2012**, *1*, N123–N126.

(5) Böscke, T.; Teichert, S.; Bräuhaus, D.; Müller, J.; Schröder, U.; Böttger, U.; Mikolajick, T. Phase transitions in ferroelectric silicon-doped hafnium oxide. *Applied Physics Letters* **2011**, *99*, 112904.

(6) Clima, S.; Wouters, D.; Adelmann, C.; Schenk, T.; Schroeder, U.; Jurczak, M.; Pourtois, G. Identification of the ferroelectric switching process and dopant-dependent switching properties in orthorhombic HfO2: A first principles insight. *Applied Physics Letters* **2014**, *104*, 092906.

(7) Asa, M.; Baldrati, L.; Rinaldi, C.; Bertoli, S.; Radaelli, G.; Cantoni, M.; Bertacco, R. Electric field control of magnetic properties and electron transport in BaTiO3-based multiferroic heterostructures. *Journal of Physics: Condensed Matter* **2015**, *27*, 504004.

(8) Haeni, J. et al. Room-temperature ferroelectricity in strained SrTiO3. *Nature* **2004**, *430*, 758.

(9) Choi, K. J.; Biegalski, M.; Li, Y.; Sharan, A.; Schubert, J.; Uecker, R.; Reiche, P.; Chen, Y.; Pan, X.; Gopalan, V.; Chen, L.; Schlom, D.; Eom, C. Enhancement of ferroelectricity in strained BaTiO3 thin films. *Science* **2004**, *306*, 1005–1009.

(10) Valencia, S. et al. Interface-induced room-temperature multiferroicity in BaTiO3. *Nature Materials* **2011**, *10*, 753.

(11) Bersch, E.; Rangan, S.; Bartynski, R. A.; Garfunkel, E.; Vescovo, E. Band offsets of ultrathin high-κ oxide films with Si. *Physical Review B* **2008**, *78*, 085114.

(12) Suzuki, K.; Kijima, K. Optical band gap of barium titanate nanoparticles prepared by RF-plasma chemical vapor deposition. *Japanese Journal of Applied Physics* **2005**, *44*, 2081.

(13) Van Benthem, K.; Elsässer, C.; French, R. Bulk electronic structure of SrTiO 3: experiment and theory. *Journal of Applied Physics* **2001**, *90*, 6156–6164.

(14) Hwang, C. S. Thickness-dependent dielectric constants of (Ba,Sr)TiO3 thin films with Pt or conducting oxide electrodes. *Journal of Applied Physics* **2002**, *92*, 432–437.

(15) Schroeder, U.; Mueller, S.; Mueller, J.; Yurchuk, E.; Martin, D.; Adelmann, C.; Schloesser, T.; van Bentum, R.; Mikolajick, T. Hafnium oxide based CMOS compatible ferroelectric materials. *ECS Transactions* **2013**, *50*, 15–20.

(16) Shimizu, T.; Katayama, K.; Kiguchi, T.; Akama, A.; Konno, T. J.; Sakata, O.; Funakubo, H. The demonstration of significant ferroelectricity in epitaxial Y-doped HfO2 film. *Scientific reports* **2016**, *6*, 32931.

(17) Schröder, U.; Yurchuk, E.; Müller, J.; Martin, D.; Schenk, T.; Polackowski, P.; Adelmann, C.; Popovici, M.; Kalinin, S.; Mikolajick, T. Impact of different dopants on the switching properties of ferroelectric hafniumoxide. *Japanese Journal of Applied Physics* **2014**, *53*, 08LE02.

(18) Tian, X.; Shibayama, S.; Nishimura, T.; Yajima, T.; Migita, S.; Toriumi, A. Evolution of ferroelectric HfO2 in ultrathin region down to 3 nm. *Applied Physics Letters* **2018**, *112*, 102902.

(19) Chernikova, A.; Kozodaev, M.; Markeev, A.; Negrov, D.; Spiridonov, M.; Zarubin, S.; Bak, O.; Buragohain, P.; Lu, H.; Suvorova, E.; Gruverman, A.; Zenkevich, A. Ultrathin Hf0.5Zr0.5O2 ferroelectric films on Si. *ACS Applied Materials & Interfaces* **2016**, *8*, 7232–7237.

(20) Florent, K.; Lavizzari, S.; Popovici, M.; Di Piazza, L.; Celano, U.; Groeseneken, G.; Van Houdt, J. Understanding ferroelectric Al:HfO2 thin films with Si-based electrodes for 3D applications. *Journal of Applied Physics* **2017**, *121*, 204103.

(21) Wang, J.; Neaton, J.; Zheng, H.; Nagarajan, V.; Ogale, S.; Liu, B.; Viehland, D.; Vaithyanathan, V.; Schlom, D.; Waghmare, U.; Spaldin, N.; Rabe, K.; Wuttig, M.; Ramesh, R. Epitaxial BiFeO3 multiferroic thin film heterostructures. *Science* **2003**, *299*, 1719–1722.

(22) Van Aken, B. B.; Palstra, T. T.; Filippetti, A.; Spaldin, N. A. The origin of ferroelectricity in magnetoelectric YMnO3. *Nature Materials* **2004**, *3*, 164.

(23) Ramesh, R.; Spaldin, N. A. Multiferroics: progress and prospects in thin films. *Nature Materials* **2007**, *6*, 21.

(24) Duan, C.-G.; Jaswal, S. S.; Tsymbal, E. Y. Predicted magnetoelectric effect in Fe/BaTiO3 multilayers: ferroelectric control of magnetism. *Physical Review Letters* **2006**, *97*, 047201.

(25) Lahtinen, T. H.; Tuomi, J. O.; van Dijken, S. Electrical writing of magnetic domain patterns in ferromagnetic/ferroelectric heterostructures. *IEEE Transactions on Magnetics* **2011**, *47*, 3768–3771.

(26) Wu, T.; Bur, A.; Zhao, P.; Mohanchandra, K. P.; Wong, K.; Wang, K.; Lynch, C.; Carman, G. Giant electric-field-induced reversible and permanent magnetization reorientation on magnetoelectric Ni/(011)[Pb (Mg 1/3 Nb 2/3) O 3](1- x)–[PbTiO 3] x heterostructure. *Applied Physics Letters* **2011**, *98*, 012504.

(27) Li, Q.; Tan, A.; Scholl, A.; Young, A.; Yang, M.; Hwang, C.; NDiaye, A.; Arenholz, E.; Li, J.; Qiu, Z. Electrical switching of the magnetic vortex circulation in artificial multiferroic structure of Co/Cu/PMN-PT (011). *Applied Physics Letters* **2017**, *110*, 262405.

(28) Bauer, U.; Emori, S.; Beach, G. S. Voltage-controlled domain wall traps in ferromagnetic nanowires. *Nature Nanotechnology* **2013**, *8*, 411.

(29) Bauer, U.; Yao, L.; Tan, A. J.; Agrawal, P.; Emori, S.; Tuller, H.; Van Dijken, S.; Beach, G. Magneto-ionic control of interfacial magnetism. *Nature Materials* **2015**, *14*, 174.

(30) Zhu, X.; Zhou, J.; Chen, L.; Guo, S.; Liu, G.; Li, R.; Lu, W. In Situ Nanoscale Electric Field Control of Magnetism by Nanoionics. *Advanced Materials* **2016**, *28*, 7658–7665.

(31) Maruyama, T.; Shiota, Y.; Nozaki, T.; Ohta, K.; Toda, N.; Mizuguchi, M.; Tulapurkar, A.; Shinjo, T.; Shiraishi, M.; Mizukami, S.; Ando, Y.; Suzuki, Y. Large voltage-induced magnetic anisotropy change in a few atomic layers of iron. *Nature Nanotechnology* **2009**, *4*, 158.

(32) Niranjan, M. K.; Duan, C.-G.; Jaswal, S. S.; Tsymbal, E. Y. Electric field effect on magnetization at the Fe/MgO (001) interface. *Applied Physics Letters* **2010**, *96*, 222504.

(33) Li, X.; Yu, G.; Wu, H.; Ong, P.; Wong, K.; Hu, Q.; Ebrahimini, F.; Upadhyaya, P.; Akyol, M.; Kioussis, N.; Han, X.; Khalili Amiri, P.; Wang, K. Thermally stable voltage-controlled perpendicular magnetic anisotropy in Mo—CoFeB—MgO structures. *Applied Physics Letters* **2015**, *107*, 142403.

(34) Nozaki, T.; Kozioł-Rachwał, A.; Skowroński, W.; Zayets, V.; Shiota, Y.; Tamaru, S.; Kubota, H.; Fukushima, A.; Yuasa, S.; Suzuki, Y. Large voltage-induced changes in the perpendicular magnetic anisotropy of an MgO-based tunnel junction with an ultrathin Fe layer. *Physical Review Applied* **2016**, *5*, 044006.

(35) Nakazawa, S.; Obinata, A.; Chiba, D.; Ueno, K. Electric field control of magnetic anisotropy in a Co/Pt bilayer deposited on a high-κ SrTiO3. *Applied Physics Letters* **2017**, *110*, 062406.

(36) Xiang, H.; Al-Mahdawi, M.; Belmoubaric, M.; Kasai, S.; Sakuraba, Y.; Mitani, S.; Hono, K. Atomic layer number dependence of voltage-controlled magnetic anisotropy in Cr/Fe/MgAl2O4 heterostructure. In Proceedings of the Intermag2018, Singapore, FC-03, Marina Bay Sands Convention Center. **2018**.

(37) Huang, Z.; Stolichnov, I.; Bernand-Mantel, A.; Borrel, J.; Auffret, S.; Gaudin, G.; Boulle, O.; Pizzini, S.; Ranno, L.; Herrera Diez, L.; Setter, N. Ferroelectric control of magnetic domains in ultra-thin cobalt layers. *Applied Physics Letters* **2013**, *103*, 222902.

(38) Mardana, A.; Ducharme, S.; Adenwalla, S. Ferroelectric control of magnetic anisotropy. *Nano Letters* **2011**, *11*, 3862–3867.

(39) Couet, S.; Bisht, M.; Trekels, M.; Menghini, M.; Petermann, C.; Van Bael, M.; Locquet, J.; Rueffer, R.; Vantomme, A.; Temst, K. Electric Field-Induced Oxidation of Ferromagnetic/Ferroelectric Interfaces. *Advanced Functional Materials* **2014**, *24*, 71–76.

(40) Bisht, M.; Couet, S.; Lazenka, V.; Modarresi, H.; Rüffer, R.; Locquet, J.; Van Bael, M.; Vantomme, A.; Temst, K. Electric Polarity-Dependent Modification of the Fe/BaTiO3 Interface. *Advanced Materials Interfaces* **2016**, *3*, 1500433.

(41) Garcia, V.; Bibes, M.; Bocher, L.; Valencia, S.; Kronast, F.; Crassous, A.; Moya, X.; Enouz-Vedrenne, S.; Gloter, A.; Imhoff, D.; Deranlot, C.; Mathur, N.; Fusil, S.; Bouzehouane, K.; Barthelemy, A. Ferroelectric control of spin polarization. *Science* **2010**, *327*, 1106–1110.

(42) Miwa, S. et al. Voltage controlled interfacial magnetism through platinum orbits. *Nature Communications* **2017**, *8*, 15848.

(43) Park, M. H.; Lee, Y. H.; Mikolajick, T.; Schroeder, U.; Hwang, C. S. Review and perspective on ferroelectric HfO2-based thin films for memory applications. *MRS Communications* **2018**, *8*, 795–808.

(44) Chernikova, A. G.; Kozodaev, M. G.; Negrov, D. V.; Korostylev, E. V.; Park, M. H.; Schroeder, U.; Hwang, C. S.; Markeev, A. M. Improved ferroelectric switching endurance of La-doped Hf0.5Zr0.5O2 thin films. *ACS Applied Materials & Interfaces* **2018**, *10*, 2701–2708.

(45) Ho, M.-Y.; Gong, H.; Wilk, G.; Busch, B.; Green, M.; Voyles, P.; Muller, D.; Bude, M.; Lin, W.; See, A.; Loomans, M.; Lahiri, S.; Raisanen, P. Morphology and crystallization kinetics in HfO 2 thin films grown by atomic layer deposition. *Journal of Applied Physics* **2003**, *93*, 1477–1481.

(46) Ohtaka, O.; Yamanaka, T.; Kume, S. Synthesis and X-ray structural analysis by the Rietveld method of orthorhombic hafnia. *Journal of the Ceramic Society of Japan* **1991**, *99*, 826–827.

(47) Canedy, C.; Li, X.; Xiao, G. Large magnetic moment enhancement and extraordinary Hall effect in Co/Pt superlattices. *Physical Review B* **2000**, *62*, 508.

(48) Vermeulen, B. F.; Wu, J.; Swerts, J.; Couet, S.; Linten, D.; Radu, I.; Temst, K.; Rampelberg, G.; Detavernier, C.; Groeseneken, G.; Martens, K. Perpendicular magnetic

anisotropy of Co\Pt bilayers on ALD HfO2. *Journal of Applied Physics* **2016**, *120*, 163903.

(49) Kittel, C. *Introduction to solid state physics*; Wiley New York, 1976; Vol. 8.

(50) Carcia, P. Perpendicular magnetic anisotropy in Pd/Co and Pt/Co thin-film layered structures. *Journal of applied physics* **1988**, *63*, 5066–5073.

(51) Vermeulen, B. F.; Wu, J.; Swerts, J.; Couet, S.; Radu, I. P.; Groeseneken, G.; Detavernier, C.; Jochum, J. K.; Van Bael, M.; Temst, K.; Shukla, A.; Miwa, S.; Suzuki, Y.; Martens, K. M. Perpendicular magnetic anisotropy of CoFeB\Ta bilayers on ALD HfO2. *AIP Advances* **2017**, *7*, 055933.

(52) Coey, J. M. *Magnetism and Magnetic Materials*; Cambridge University Press, 2010.

(53) Bertero, G.; Sinclair, R.; Park, C.-H.; Shen, Z. Interface structure and perpendicular magnetic anisotropy in Pt/Co multilayers. *Journal of Applied Physics* **1995**, *77*, 3953–3959.

(54) Bandiera, S.; Sousa, R.; Rodmacq, B.; Dieny, B. Enhancement of perpendicular magnetic anisotropy through reduction of Co-Pt interdiffusion in (Co/Pt) multilayers. *Applied Physics Letters* **2012**, *100*, 142410.

(55) Pustogowa, U.; Zabloudil, J.; Uiberacker, C.; Blaas, C.; Weinberger, P.; Szunyogh, L.; Sommers, C. Magnetic properties of thin films of Co and of (CoPt) superstructures on Pt (100) and Pt (111). *Physical Review B* **1999**, *60*, 414.

(56) Nistor, L.; Rodmacq, B.; Auffret, S.; Dieny, B. Pt/Co/oxide and oxide/Co/Pt electrodes for perpendicular magnetic tunnel junctions. *Applied Physics Letters* **2009**, *94*, 012512.

(57) Lomenzo, P. D.; Takmeel, Q.; Zhou, C.; Fancher, C. M.; Lambers, E.; Rudawski, N. G.; Jones, J. L.; Moghaddam, S.; Nishida, T. TaN interface properties and electric field

cycling effects on ferroelectric Si-doped HfO2 thin films. *Journal of Applied Physics* **2015**, *117*, 134105.

(58) Park, M. H.; Kim, H. J.; Kim, Y. J.; Lee, Y. H.; Moon, T.; Kim, K. D.; Hyun, S. D.; Hwang, C. S. Study on the size effect in Hf0.5Zr0.5O2 films thinner than 8 nm before and after wake-up field cycling. *Applied Physics Letters* **2015**, *107*, 192907.

(59) Grimley, E. D.; Schenk, T.; Sang, X.; Pešić, M.; Schroeder, U.; Mikolajick, T.; LeBeau, J. M. Structural Changes Underlying Field-Cycling Phenomena in Ferroelectric HfO2 Thin Films. *Advanced Electronic Materials* **2016**, *2*, 1600173.

(60) Schenk, T.; Hoffmann, M.; Ocker, J.; Pesic, M.; Mikolajick, T.; Schroeder, U. Complex internal bias fields in ferroelectric hafnium oxide. *ACS Applied Materials & Interfaces* **2015**, *7*, 20224–20233.

(61) Starschich, S.; Menzel, S.; Böttger, U. Evidence for oxygen vacancies movement during wake-up in ferroelectric hafnium oxide. *Applied Physics Letters* **2016**, *108*, 032903.

(62) Dobrotă, C.-I.; Stancu, A. What does a first-order reversal curve diagram really mean? A study case: Array of ferromagnetic nanowires. *Journal of Applied Physics* **2013**, *113*, 043928.

(63) Siadou, N.; Androutsopoulos, M.; Panagiotopoulos, I.; Stoleriu, L.; Stancu, A.; Bakas, T.; Alexandrakis, V. Magnetization reversal in [Ni/Pt] 6/Pt (x)/[Co/Pt] 6 multilayers. *Journal of Magnetism and Magnetic Materials* **2011**, *323*, 1671–1677.

(64) Shiota, Y.; Maruyama, T.; Nozaki, T.; Shinjo, T.; Shiraishi, M.; Suzuki, Y. Voltage-assisted magnetization switching in ultrathin Fe80Co20 alloy layers. *Applied Physics Express* **2009**, *2*, 063001.

(65) Song, C.; Cui, B.; Li, F.; Zhou, X.; Pan, F. Recent progress in voltage control of

magnetism: Materials, mechanisms, and performance. *Progress in Materials Science* **2017**, *87*, 33–82.

(66) Hu, J.-M.; Chen, L.-Q.; Nan, C.-W. Multiferroic heterostructures integrating ferroelectric and magnetic materials. *Advanced Materials* **2016**, *28*, 15–39.

(67) Sahoo, S.; Polisetty, S.; Duan, C.-G.; Jaswal, S. S.; Tsymbal, E. Y.; Binek, C. Ferroelectric control of magnetism in BaTiO3/Fe heterostructures via interface strain coupling. *Physical Review B* **2007**, *76*, 092108.

(68) Wu, S.; Cybart, S. A.; Yu, P.; Rossell, M.; Zhang, J.; Ramesh, R.; Dynes, R. Reversible electric control of exchange bias in a multiferroic field-effect device. *Nature Materials* **2010**, *9*, 756.

(69) Wu, S.; Cybart, S. A.; Yi, D.; Parker, J. M.; Ramesh, R.; Dynes, R. Full electric control of exchange bias. *Physical Review Letters* **2013**, *110*, 067202.